Compton Scattering: Light reveals its particle nature

Simon Lacoste-Julien
Mathieu Plamondon

Lab Report
Department of Physics
McGill University

February 4, 2002

Abstract

Incident gamma rays from a ^{137}Cs source are scattered from an aluminum target and the spectrum at various angles is taken with a NaI scintillator detector. By evaluating the energy corresponding to the peaks of the number of counts, the Compton formula for the frequency shift can be validated. Further investigations of the differential cross-section allow discrimination between the classical approach and the quantum-mechanical one.

1 Introduction

Early in the 20^{th} century, many successful theories established that interactions between electromagnetic radiation of frequency ν and matter occur through the emission or absorption of discrete quanta of energy $E = h\nu$. This idea, initiated by Planck[1], solved the problem of the blackbody spectrum (1901). It was also shown later that the explanation of the photoelectric effect (Einstein, 1905) and the hydrogen spectrum (Bohr, 1913) required such redefinition of light.

In 1920, an American physicist named Arthur H. Compton decided to investigate another phenomenon which classical physics failed to explain. Its experiments on monochromatic X-rays scattered from various materials revealed that their energy (frequency) was decreased after the scattering. Classical electromagnetic theory couldn't explain this frequency shift because frequency is a property of the electromagnetic wave and cannot be altered by the change of direction implied by the scattering[2]. On the other hand, we can explain this result by considering light as a beam of photons which undergo elastic collisions with the electrons in the material (as explained in section 2.1). Compton demonstrated in 1923 [8, p.231] a complete agreement between his experimental results and the predictions from the quantum theory of light, giving rise to one of the most impressive successes of quantum theory.

We will describe the results of a similar experiment in this paper. We have studied the angular energy dependence of gamma rays (from ^{137}Cs) scattered by electrons in an aluminum target. Our goal wasn't restricted to verify historical successes of Quantum Mechanics. Implicitly, such laboratory work is an excellent introduction to modern experimental methods. For the purpose of this experiment, our main objective was to discriminate between the classical treatment of the Compton scattering phenomenon (Thomson cross-section and no angular dependence for frequency) and the quantum-mechanical one (Klein-Nishima and Compton scattering formula).

2 Theory

2.1 The Compton Effect

We consider the situation where γ-rays are incident to a metal. As mentioned in the introduction, Compton explained the decrease of their energy after being scattered (called the *Compton Effect*) by treating the incoming radiation as quanta of light with energy $h\nu$ and momentum $h\nu/c$, where ν is their frequency, as proposed by Einstein. Indeed, we can then consider the interaction of light with the electrons in the metal as a simple collision of particles and apply the classical relativistic conservation laws.

First of all, we can neglect the binding energy of the electrons in the metal compared to the γ-ray energy, and thus treat them as essentially free. Similarly,

[1] see [2] for example
[2] see, for example, chapter 10 of [5]

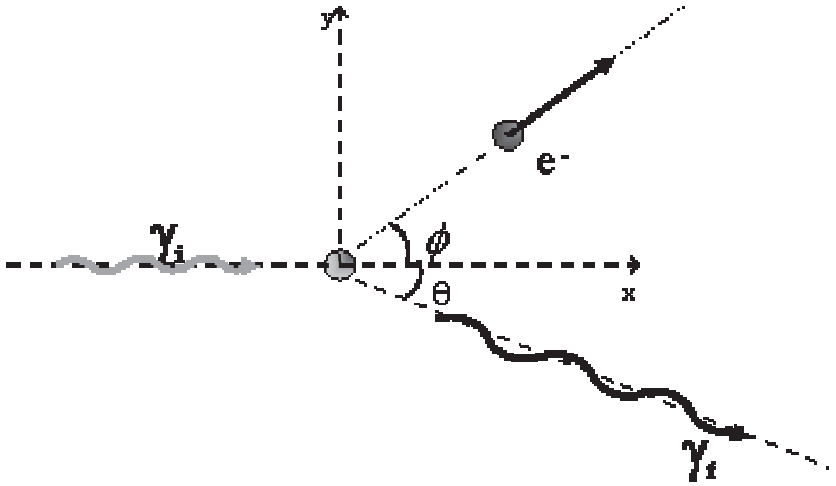

Figure 1: **Compton scattering of a photon from a free electron**

we can assume that their momentum in the lab frame is negligible compared to the one of incident photons. The interaction between a photon and an electron is then as shown in figure 1: γ_i represents the incident photon, γ_f represents the scattered photon which makes an angle θ with the x-axis and e^- is the scattered electron.

So let p_i and p_f be the momentum of the incident photon and scattered photon respectively, E_i and E_f be their energy; and let m be the mass of the electron and p_e its momentum after the collision. Energy conservation can then be expressed as:

$$E_i + mc^2 = E_f + \sqrt{(mc^2)^2 + (p_e c)^2} \tag{1}$$

Also, momentum conservation requires that

$$\vec{p_i} = \vec{p_f} + \vec{p_e} \tag{2}$$

Square $\vec{p_e}$ in Equation (2) to obtain

$$p_e^2 = (\vec{p_i} - \vec{p_f}) \bullet (\vec{p_i} - \vec{p_f}) = p_i^2 + p_f^2 - 2p_i p_f cos\,\theta \tag{3}$$

Next, we multiply both sides of Equation (3) by c^2 and replace $p_i c$ and $p_f c$ by E_i and E_f. Thus

$$(p_e c)^2 = E_i^2 + E_f^2 - 2E_i E_f cos\,\theta \tag{4}$$

Now, we get another expression for $(p_e c)^2$ by squaring the square root part of Equation (1):

$$(p_e c)^2 = E_i^2 + E_f^2 + 2mc^2(E_i - E_f) \tag{5}$$

Finally, by equating expressions (4) and (5) and rearranging, we arrive to the result

$$\frac{1}{E_f} - \frac{1}{E_i} = \frac{1}{mc^2}(1 - cos\,\theta) \tag{6}$$

which is the equation we'll use in this lab; but the **Compton scattering equation** is more often written in terms of the change of wavelength $\Delta\lambda$, using the relationship $\lambda = h/E$:

$$\Delta\lambda = \frac{h}{mc^2}(1 - cos\,\theta) \tag{7}$$

which expresses the change in wavelength of the γ-ray in terms of its recoil angle θ and the **Compton wavelength** $\frac{h}{mc^2}$, as defined for an electron of mass m.

From the Compton equation, we can notice that the change of wavelength is independent of the wavelength of the incident photon, and that this change is proportional with the Compton wavelength. Even for very light electrons, the Compton wavelength is quite small, 2.42×10^{-3} nm, compared with the wavelength of visible light. This means that the fractional change in wavelength by Compton scattering is only substantial for X-rays or γ-rays. In this experiment, we use γ-rays from a ^{137}Cs source which have an energy of 662 KeV and scatter on electrons with rest mass (energy) of 511 KeV, so that the energy of the scattered photon at an angle of 90^o should be shifted to 288 KeV. This is indeed a noticeable shift, and was observed during our experiment.

2.2 Cross-Section

Next we are interested in the differential cross-section for the scattering of the radiation from the electrons. Differential cross-section is defined as usual by

$$\frac{d\sigma}{d\Omega} = \frac{\text{\# of particles detected in a direction / unit time-unit solid angle}}{\text{\# of incident particle / unit area-unit time}} \tag{8}$$

or in the case of radiation,

$$\frac{d\sigma}{d\Omega} = \frac{\text{power radiated in specific direction / unit solid angle}}{\text{power incident / unit area}} \tag{9}$$

The classical (nonrelativistic) derivation using the power radiated by the accelerated electrons is given in [7], p. 255. We only state here the final result, namely the **Thomson differential cross-section**:

$$\frac{d\sigma}{d\Omega} = r_0^2 \left(\frac{1 + cos^2\,\theta}{2}\right) \tag{10}$$

in the direction θ from the direction of propagation of the incoming wave, and r_0 is the so-called "classical electron radius", $r_0 = 2.82 \times 10^{-13}$ cm.

The quantum-mechanical calculation adds a correction factor which shows up in the so called **Klein-Nishina formula** (see [4], p.219)

$$\frac{d\sigma}{d\Omega} = r_0^2 \frac{1+cos^2\,\theta}{2} \frac{1}{[1+\gamma(1-cos\,\theta)]^2} \times \left[1 + \frac{\gamma^2(1-cos\,\theta)^2}{(1+cos^2\,\theta)[1+\gamma(1-cos\,\theta)]}\right] \tag{11}$$

where r_0 and θ were defined previously, and $\gamma = E_i/mc^2$ (with same variables as in equation (1)). A comparison of the Thomson (10) and Klein-Nishina (11) cross-sections, including the results obtained in this laboratory for $\gamma = 1.29$, is shown in Figure 10 on page 19.

Experimentally, the Compton cross-section can be obtained by:

$$\frac{d\sigma}{d\Omega} = \frac{yield}{(d\Omega)NI_0} \tag{12}$$

where *yield* is the number of hits per second reaching the detector in a specific direction[3], N is the total number of electrons in the target which lie in the path of the incident beam and I_0 is the flux density of γ-rays at the target [7, p. 264]. How we can use this equation in our experiment will be explained in section 4.2 in the **Data and analysis** section.

3 Experiment

3.1 Setup

The experimental setup is shown in figure 2 and can be visualized in the following sequence. A radioactive ^{137}Cs source produces 662 KeV γ-rays which can escape the shielded cavity only through a small hole. The beam created is collimated and reaches an aluminum rod (the target). Some portion of the γ-rays are scattered by the electrons in the target according to the Compton Effect described in section 2. By rotating the circular basis, the NaI scintillator can detect these radiations at various angles. Though the detector will be described thoroughly in section 3.2, for now we can say that the effect in the detector will be a current pulse with amplitude proportional to the energy of the incoming radiation. The signal is converted and amplified to a compatible voltage for the PCA card of the computer which has to discriminate the amplitudes into 2048 intervals, each pulse increasing the count in the so called channels. The PCA-II software from Nucleus analyzes this data and produces a live spectrum on the screen, which we can now browse to find peaks, area under curve, etc.

[3]Note that this is usually not what you can read directly from your spectrum since no detector can detect all the incoming photons; they only detect a constant fraction of it (called its **efficiency factor**) depending on their energy.

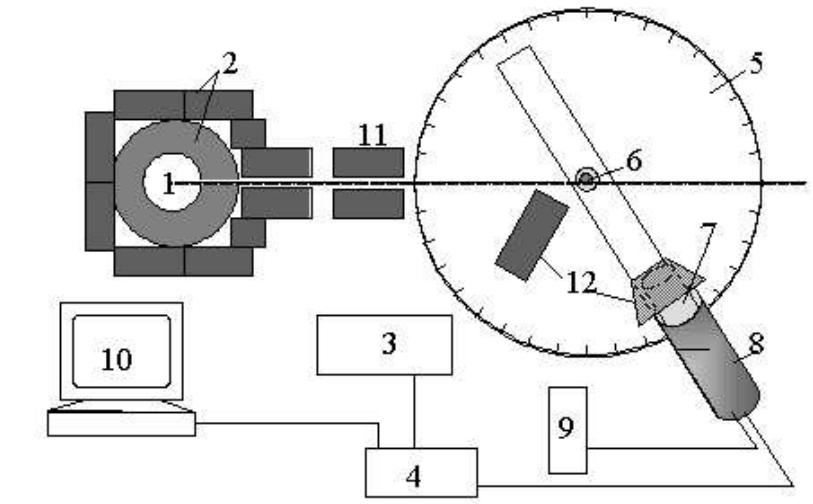

1. ^{137}Cs Source 4. Amplifier 7. NaI scintillator 10. Data acquisition computer
2. Lead shield 5. Rotating base 8. Photomultiplier 11. Additional collimation
3. Oscilloscope 6. Aluminum target 9. Power supply 12. Lead stopping rays from the mouth of the collimation

Figure 2: **Experimental Setup**

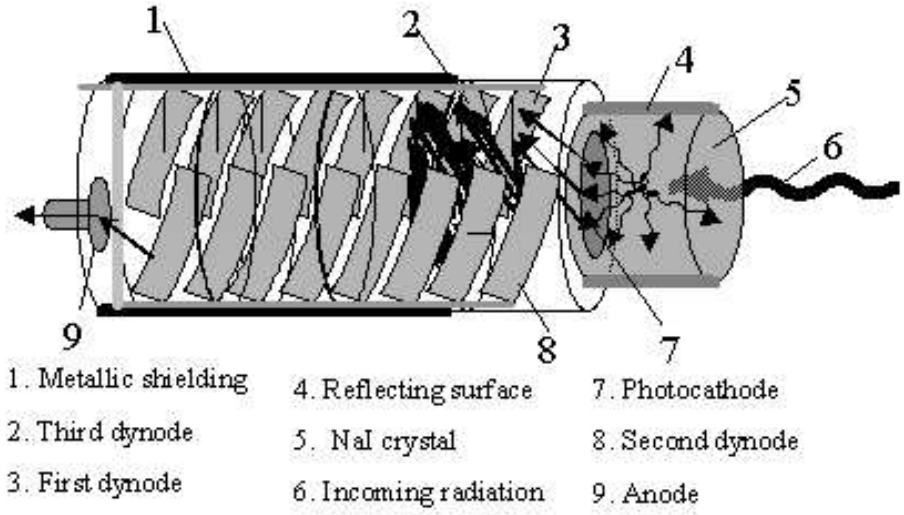

Figure 3: **NaI Scintillation Detector**

3.2 Detector

Considering its strong links with the statistical errors (see section 4.1.4), our detector deserves a thorough description of its functioning [1, p.13]. Figure 3 represents the schematic processes involved in the transformation of an incident radiation into a current pulse. Enclosed in a light-proof box, the system is composed of two parts: a scintillator and a photomultiplier. The first one, a 2"diameter x 2" cylindrical crystal of NaI(Ti), receives the incident ionizing photon of energy E. The latter dissipates its energy in the excitation of the electrons which are rapidly stopped in the material. Hence, a fraction of E is converted into N photons radiated in all directions, as seen in the picture.

The surrounding reflector maximizes the number of these photons which fall on the photocathode and extract electrons from it by photoelectric effect. The photo-electrons are accelerated by the potential applied between the cathode and the first dynode of the photomultiplier and strike it, ejecting more electrons in the same way. This multiplication process is repeated at subsequent dynodes, each one being at a higher potential than the previous one. In the end, such an electrons avalanche produces a current pulse at the anode which is transformed after. In our experiment, the determination of the response N of the scintillator as a function of E enables the instrument to be calibrated for use as a spectroscope. Such curve giving the efficiency comes with the apparatus. A last note concerns the presence of magnetic fluctuations in every physics lab. Their origins can vary from the nearby wires to the magnetic field of the Earth,

but their altering effects during the accelerations in cascade are diminished by a metallic shielding around the photomultiplier.

3.3 Procedure

With a single series of spectra for several angles, the analyst has more or less all the material needed in order to achieve this experiment (see section 4.1). The evaluation of the position of the peaks allows to verify the Compton's hypothesis while the number of counts under these peaks is related to the differential cross-section. However, some preliminary settings have to be accomplished before these results become in a sense worthy. The first and crucial step consists in a systematic calibration before each set of measures, i.e. to know the energy associated to each channel at that time. A day-to-day drifting in the detector calibration was observed through sporadic variations in the peaks' positions. Four radioactive sources provided five peaks of known energy: 511 KeV for the ^{22}Na[4], 81 and 356 KeV for the ^{133}Ba, 122 KeV for the ^{57}Co and 662 KeV for the ^{137}Cs [3]. Since these cesium rays were the more energetic to be detected, the voltage gain imposed to each pulse by the amplifier was adjusted in order to have this peak sitting in the far right of our spectrum screen.

Precision requires a second conscientious measure: the evaluation of the zero angle. Unfortunately, a direct measurement at small angles could be fatal to our detector which cannot endure the high intensity of the principal beam. We resolve this problem by using the symmetry of the Compton relation about $\theta = 0$. We set an arbitrary 0 by eye; we then measure the channel number of the Compton peak at 40^o to the right, say; and then we try to find at which angle to the left we obtain exactly the same peak. It appeared that the setting by eye was pretty good, so that the symmetric peak was found to be around 41^o to the left; the angle 0 is then simply in the middle of those two angles.

The data gathering itself was influenced by a marked presence of the background. When any spectral measure was achieved, a systematic spectrum without scatterer was taken at the same angle. Such treatment is imposed by the peculiarities of the background like its asymmetry. Typical series of measurements contain couples Compton peak-background: a fixed period of 300 seconds for each and angles increasing by steps of 40^o , ranging from 20^o to 120^o. In addition to the lead shielding (see figure 3) which stops the photons scattered from the mouth of the collimator, the detector is placed relatively far from the principal beam in order to minimize the proportion of background radiation. Although this choice sacrifices a good part of the intensity, it provides advantages like more precise definitions of the angle of scattering and the solid angle with respect to the scintillator's dimensions. Also, it avoids the danger of the piling effect which consists in a superimposition of simultaneous pulses and an increased energy for the signal.

[4]Note that this peak for Na wasn't found in [3], but was given by Professor Buchinger.

4 Data and Analysis

4.1 Mass of Electron

Using the spectra of the γ-ray radiation scattered at different angle by the aluminum rod, we can find the angular dependence of their energy peaks, and thus verify the Compton scattering equation (6) (by computing the mass of the electron with a fit of the Compton equation). Because of the lack of resolution of our detector, the presence of background noise and the varying efficiency of the detector, the systematic determination of the energy peaks of the spectra appeared to be a very challenging task. For ease of analysis, we have saved in ASCII format all the spectra recorded with the Nucleus PCA-II software and we have imported them in a (huge) Excel spreadsheet. This was useful for comparing the different spectra and to compare different methods of peak analysis.

4.1.1 Calibration

Our first approach for the peak analysis was to read directly by eye the channel numbers of the energy peaks on the PCA-II software for each spectrum. Using the known energies for the peaks of Ba, Co, Cs and Na, we could obtain a relation channel/energy. This was found to be pretty linear, (as expected by the manufacturer specifications of the card) and was similar to the one presented in figure 4. In fact, the data presented in figure 4 was not determined by eye but using systematic Gaussian fit, as we will explain in section 4.1.4. But the point here is that there wasn't much difference (to the eye) between the two.

4.1.2 Background

Typical untreated spectra are shown in figure 5. These two spectra were taken at 30^o, and the lower one is the background which was recorded after taking out the aluminum rod (for the same amount of time). We can see the presence of a significant background in the range of channels 1250-1500 (which correspond to around 500 KeV with our calibration). This causes a slight shift of the peak to the left, so we needed to subtract the background to the original spectrum[5] to obtain the correct peak (and correct cross-section for the analysis in section 4.2). We have taken a background spectrum at each different angle since it was changing. To get more insight in what causes some parts of the background, we have depicted its evolution in comparison with the Compton spectra in figure 6. From this plot, we can see that the background was more important at small angles and at big angles. We also see[6] that a 'ghost' back-

[5] Strictly speaking, we are combining two events which have little in common, but we assume that the background contribution in one spectrum can be *statistically* cancelled by subtracting the background alone. For better results, we should really make an average over a long period of time (or lots of trials). Due to time constraint, we couldn't do that...

[6] Well, it is not really obvious from this plot; but with the magic of computers, we can zoom in and browse different spectra to arrive to this conclusion...

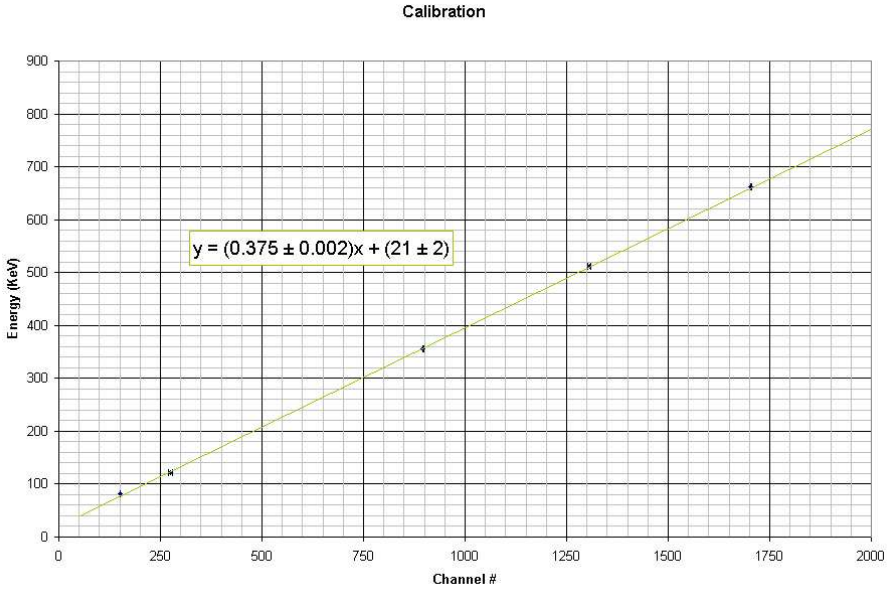

Figure 4: **Calibration relationship between channels and energy.** The energy peaks were found from the calibration spectra after background and efficiency corrections. The error bars are pretty small because of the accuracy of the Gaussian fits used to determine the Compton peaks.

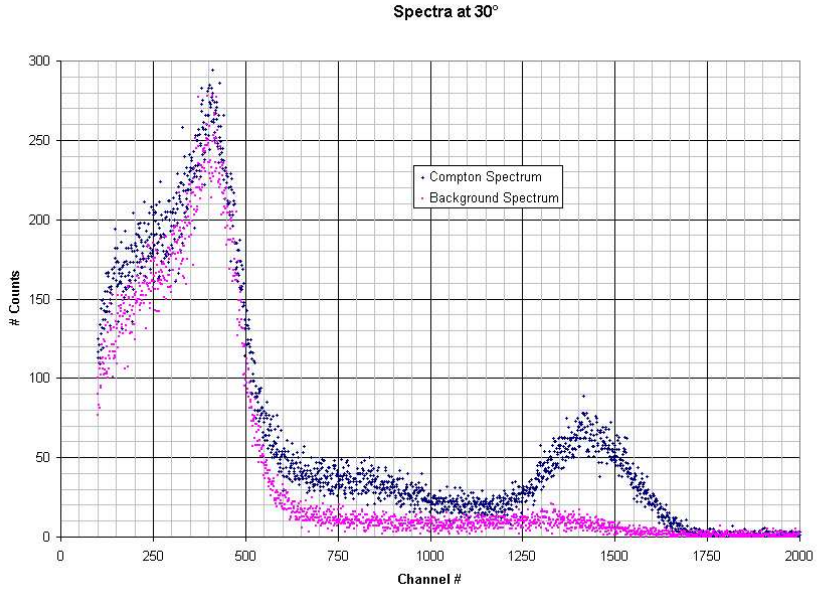

Figure 5: **Compton scattering spectrum with its corresponding background spectrum.** They were each taken over a period 30 seconds, at 30° to the right.

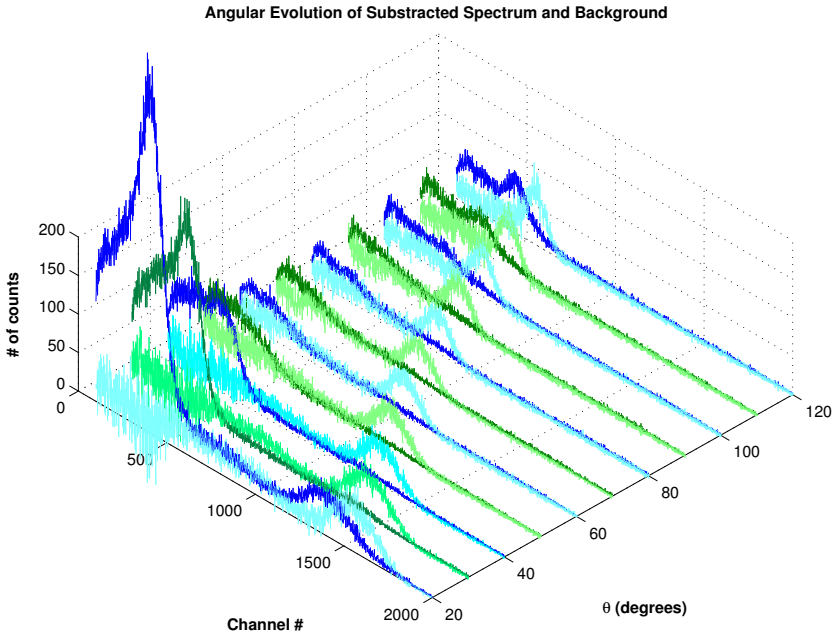

Figure 6: **Substracted Compton spectra vs. background for all our measurements.** The Compton spectra are light colored; the background ones are dark colored. All spectra were taken over periods of $300s$.

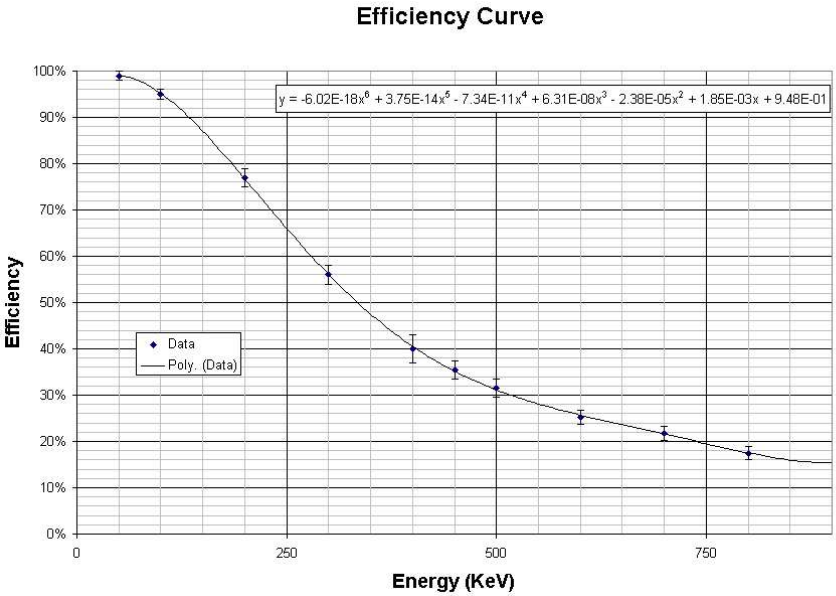

Figure 7: **Efficiency of the detector in function of incident radiation.** The error bars (and the data) were taken from the lab manual.

ground peak is always preceding the Compton peak to the left (smaller energy), and with an observable intensity at small and big angles. Since the energy of this 'ghost' peak is changing with the angle of the detector, it should be due to some kind of scattering phenomenon very similar to the one we were studying. Our hypothesis is that it was caused by some Compton scattering in the metallic screw that was fixing the rotating basis... Indeed, the vertical difference between the detector and the screw increases slightly the angle of scattering, which could explain why the 'ghost' peak is a bit less energetic than our Compton peak. Unfortunately, we thought about this too late to be able to test it experimentally (by hiding the screw, for example).

4.1.3 Detector efficiency

Apart the background, we needed to take the efficiency of the detector in consideration, that is, the percentage of incident photons per unit time it could detect in function of their energy. The data for the detector efficiency was taken from the lab manual; and for ease of analysis, we have fitted (using least squares) a 6^{th} degree polynomial through 9 points in the range 50-800 KeV using Excel. This fit is shown together with the polynomial in figure 7. An analyzed spectrum (for comparison of different effects) is shown in figure 8. This shows the most extreme effect of the efficiency correction amongst all angles since the

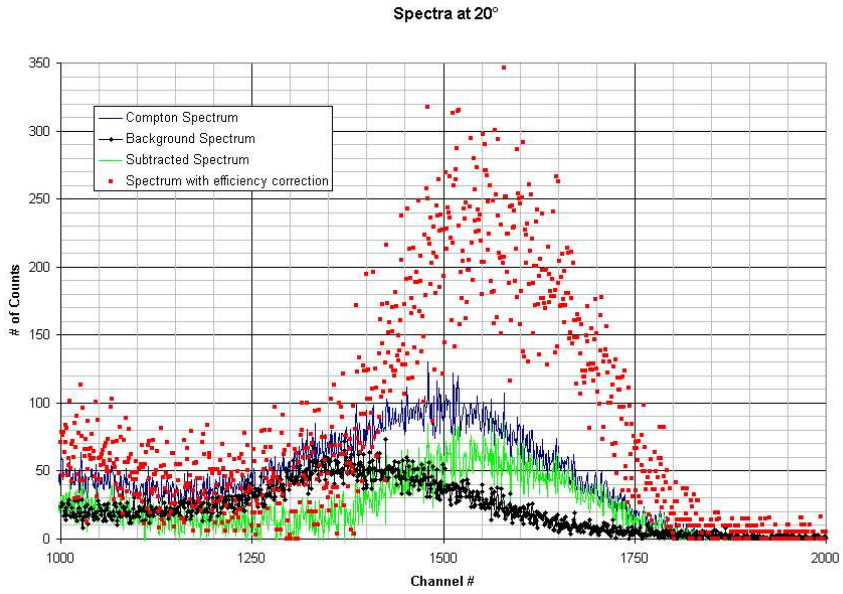

Figure 8: **Spectrum at** 20^o **and its corrections.**

variation of efficiency is more pronounced for high energies. This asymmetry in efficiency correction caused a shift to the right of all energy peaks from 10 channels for small angles to 5 channels for big angles. On the other hand, we had estimated our eye precision to determine the Compton peak on the screen of the PCA-II software to be roughly 20 channels, so we couldn't really notice this effect on the screen. So how then can we say that the energy peaks were shifted by 10? Well, this will be explained in the next section... Just before we skip to this important point, note that the efficiency was *crucial* to have a meaningful graph of the cross-section (table 2 in appendix A shows the difference in the total number of counts under the peaks with and without considering efficiency correction).

4.1.4 Systematic measure of peaks using Gaussians

We wanted to find a systematic way to localize the Compton peaks in the recorded spectra for two reasons. First, since we did measurements over short periods of time (due to time constraints), the peak shape wasn't really well-defined and we had a lot of freedom to 'choose' the channel number of the peak (and also because of the significant size of the FWHM[7] of the peak due to lack of resolution of the NaI detector). Second, the peak was polluted with background

[7] *Full Width at Half Maximum*

noise (even after substraction of the background spectrum) so we were puzzled about how we could evaluate the total number of counts for the Compton peak alone (for section 4.2). Following a 'Central-Limit' intuition, we assumed that the real Compton peak should be shaped as a Gaussian. We thus decided to fit the upper portion of each peak with a Gaussian. We used nonlinear least-squares data fitting by the Gauss-Newton method with the `nlinfit` function of Matlab. A spectacular fit of the 356 KeV peak of the Ba spectrum (which received the efficiency correction) is shown in figure 11 in appendix A. It succeeds to avoid the very close 303 KeV peak by fitting data only on an interval where most of the points are higher than 70% of the maximum number of counts. Except for this exception (Barium), all the other fits were done in the 30% and higher region. The choice of the interval over where we fit the Gaussian was a bit arbitrary, but the effect is small compared to the error made on the fit. This is discussed in appendix A together with the Matlab code we used to make our Gaussian fits. The Compton peak channel number is found using the average of the Gaussian (which is one of its parameter) and its error is estimated using the 95% confidence interval on the parameters of the Gaussian (given by the function `nparci` in Matlab).

Now, a subtle point needs to be mentioned. Because the calibration was very important for our experiment, we have done a kind of perturbation theory to evaluate it more precisely. Indeed, the efficiency correction could modify for about 10 channels the position of the calibrating peaks, so we wanted to take it into consideration. But to properly modify the counts per channel of the calibrating spectrum, we first need the relationship channel/energy since the efficiency relation is given in function of energy. So we found a first approximation to the calibration by finding the peaks with Gaussian fits of the calibrating spectra without efficiency correction (but *with* the background correction); then we used this 'first order' calibration to do the efficiency correction on the calibrating spectra and find a better evaluation of the energy peaks position. The statistical error on the slope was indeed reduced by half with this second order operation (and this is the data which was shown in figure 4).

4.1.5 Compton scattering equation verification

After having determined the Compton peaks, we could plot $1/E_f$ vs. $(1-cos\,\theta)$ to verify equation (6) (the inverse of the slope should give the mass of the electron and the inverse of the y-intercept should give the initial energy of the incoming photons). Two sets of data are presented in figure 9: one found from our quick evaluation by eye; the other derived with the Gaussian fit analysis (but both used the Gaussian fit calibration with efficiency correction). Both gave pretty good linear results (shown in table 1), truly confirming the Compton scattering equation.

Note that we didn't take in consideration the energy peak at 20° and at 120° in our least square fit. We can easily see that they fall quite far from the fit for the data determined at eye, at least (see figure 9). We can justify this choice by looking back at the subtracted spectrum vs. background evolution in figure 6.

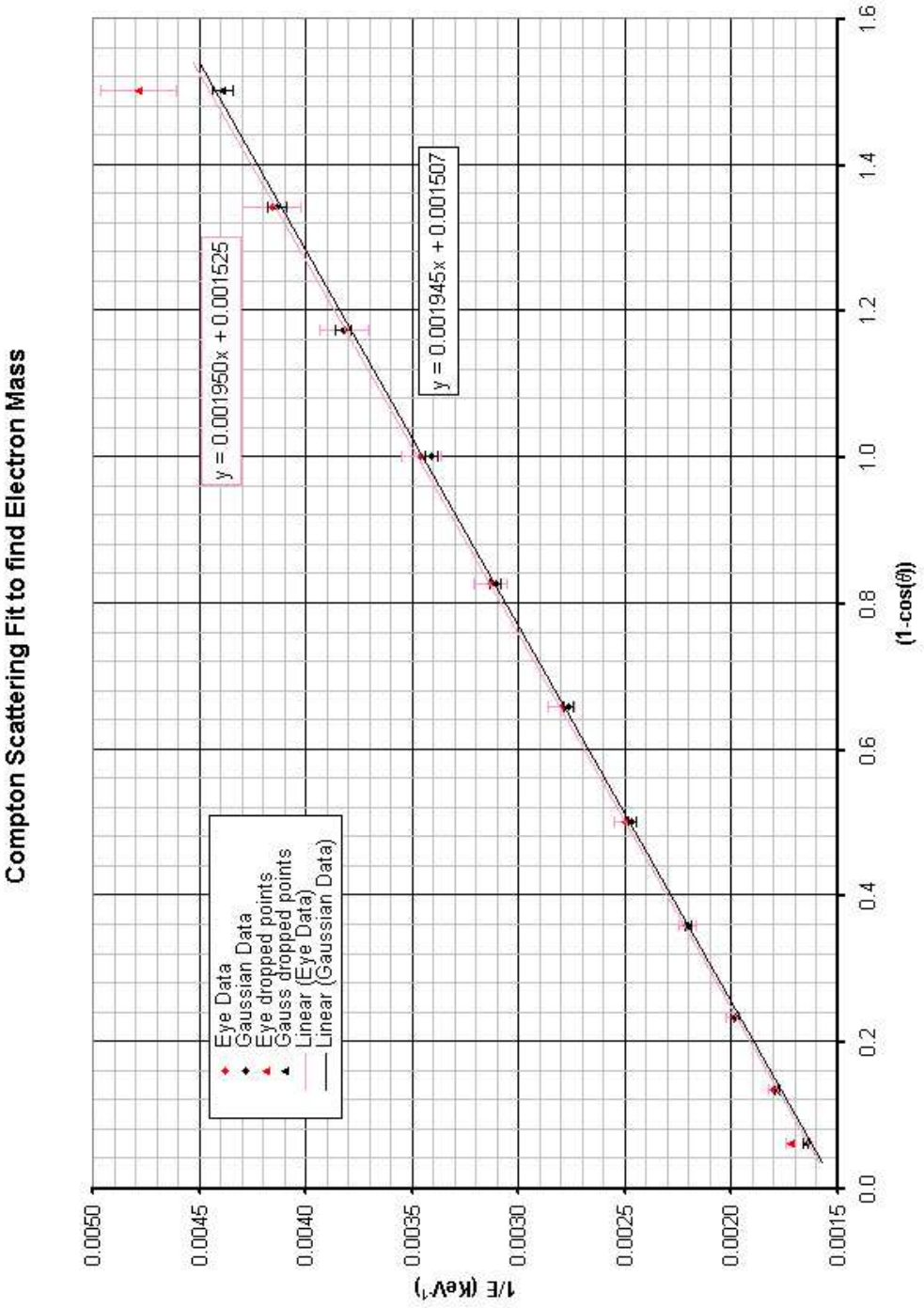

Figure 9: **Verification of Compton scattering equation.** The red fit was for data determined by eye; the black one from Gaussian fits; the data at 20° and 120° were excluded in the fit because of their questionable accuracy.

'Eye' Data	value	% error with accepted value
electron mass	513 ± 3	0.4%
energy of γ_i	656 ± 4	0.9%
Gaussian Data	value	% error with accepted value
electron mass	529 ± 2	3.5%
energy of γ_i	659 ± 2	0.4%

Table 1: **Experimental results to verify Compton scattering equation** The accepted value of the electron mass is 511 KeV and the γ_i incident energy is 662 KeV. Gaussian Data is the results derived from Gaussian fits of Compton peaks (with the background spectrum subtracted and the efficiency correction) whereas 'Eye' Data was derived from our first direct location of the peaks with the PCA-II software.

We see that at 20° and at 120°, the background and the subtracted spectrum are overlapping (and they are only significantly overlapping at those angles). This means that the background influence in the position of the peak was very strong at those angles, and that the simple substraction of the background to the raw spectrum couldn't be enough to get truly rid of the background contribution there, since we didn't do long averages. We can thus expect to have less worthy results there, and are justified to get rid of them if they don't fit well compared to the others.

The errors given in table 1 are only statistical errors derived from the slope. They are pretty small, since our linear relationship was well satisfied. Unfortunately, the accepted value for the electron mass doesn't fall into the error interval around our result derived from the Gaussian data. Interestingly enough, figure 9 shows that the Gaussian data falls into the error interval around the data that was determined by eye (the errors were derived from the ± 20 channels indetermination estimate and the statistical error on the calibration). So, by considering generous errors bars, we can reach the accepted value. On the other hand, various ways to analyze the data with Gaussian (as is shown in appendix A) yield all results close to 526 KeV, with very small statistical error, so we could conclude that our first result of 513 KeV was a lucky one... Also, the smaller error on the γ-ray energy for Gaussian analysis indicates that we should thrust more these results. Finally, even if we do a χ^2 analysis to consider the errors made on the data in the error on the slope of the fit, we get still farther away (532 ± 6 KeV). So, to summarize, our electron mass is far from the accepted value considering its very small statistical error, and we can hardly make it better... So this points towards a hidden systematic error on our results.

We tried to find a source of systematic error which could explain a higher

mass of electron, but we haven't succeeded to find a convincing one. We have thought about background radiation, efficiency shift, misplacement of angle 0, nonzero energy of the electron; but none could really explain the difference. We were forced to admit that we were clueless in face of this result: we had the weird combination of a very precise statistical result which makes the (small) absolute difference with the accepted value look very big!

4.2 Cross-section analysis

Our other goal was to discriminate between the Thomson cross-section model [eq. (10)] and the Klein-Nishina one [eq. (11)] for the Compton scattering experiment. Our results were a lot more encouraging here!

We now refer back to equation (12) on page 5 which can be used to compute the differential cross-section from experimental data. The *yield* can be calculated as follows

$$yield = \frac{1}{\Delta t} \sum_i \frac{c_i}{Eff(c_i)} \tag{13}$$

where Δt is the recording time of the computer, c_i is the number of counts recorded at channel i, $Eff(c_i)$ is the efficiency of the detector corresponding to this channel (by using the calibration relation to find the corresponding energy) and where we are summing over all the counts *corresponding to the Compton peak*. This last requirement means that we don't want to consider background noise or other peaks in this sum. This is where our Gaussian fit appears the most useful: we can simply integrate the Gaussian to obtain the total number of counts corresponding to this Compton peak. This systematic treatment of the spectra made the true relationship between the cross-section and the angle really apparent (see figure 10). In practice, we have summed over the interval of two standard deviations around the peak position. Since the percentage of area in this region is constant for any Gaussian (roughly 95%), this amounts to multiply the *yield* by a constant. The sum was quite sensitive on which fraction of the peak we were using of the peak. We have estimated the error on the sum using the standard deviation on the 5 sums obtained using 5 different fractions of the peak for the fitting (see table 2 in appendix A).

For the purpose of the discrimination between Thomson and Klein-Nishina, we didn't need the true value of the differential cross-section. So since $d\Omega = A/r^2$ where A is the cross area of the detector and r is its distance to the scatterer, we have that $d\Omega$, N and I_0 are constants in equation (12). This means that the we can simply normalize the *yield* computed to compare it with the Klein-Nishina formula. So we have plotted $\frac{d\sigma}{d\Omega}\frac{1}{r_0^2}$ vs. angle in figure 10. The normalization constant was found using least square fitting of our data by the Klein-Nishina function. We have used again the `nlinfit` function in Matlab. The complete agreement between the experimental behavior of cross-section and the quantum-theoretical one is completly apparent on this figure.

We could use the normalization constant found to deduce the incident flux intensity I_0 and compare it with some direct measurement of it. Since the

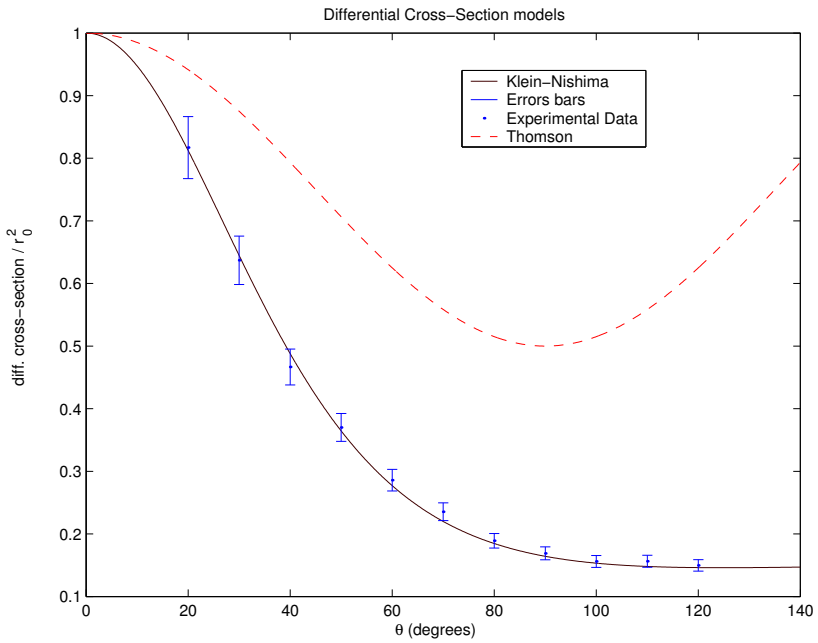

Figure 10: **Angular dependance of differential cross-section for different models.** The errors estimate we used were determined by first computing the standard deviation on the summation under the peaks using different Gaussian models (see table 2) and then using them as an estimate for our error for trial. For more uniform error estimate, we average the found relative errors over all angles and use it as our error estimate. The normalization constant was 88689 (i.e. we have divided our Gaussian integrals by 88689 to fit them with Klein-Nishina relationship.)

source was too strong, we had to put a small flat piece of lead in front of the detector to be able to measure the incident spectrum at the angle 0. Using the known attenuation relationship of the gamma rays through lead in function of thickness[8], we could in principle estimate the incident flux intensity. Some geometrical arguments should also be used to compute N, the number of electrons in the target crossed by the incident beam. Unfortunately, we haven't had the time to analyze this part of the experiment. So we just leave it here as something that could be done in the future.

5 Conclusion

Our main objective was to discriminate between the classical model and the relativistic-quantum-mechanical one for the Compton scattering phenomenon. The truly linear relationship verifying the Compton scattering equation shown in figure 9 and the very clear agreement between the experimental cross-section and the Klein-Nishina equation (shown in figure 10) have accurately answered this question. In order to analyze accurately the data, we needed to develop some systematic way to evaluate the Compton peaks, and this was done using Gaussian fits in Matlab. The background signal and the efficiency of the detector were taken in consideration in our analysis. Some interesting patterns appeared in the background signal, and we have suggested as hypothesis that it was caused by Compton scattering in the metallic screw fixing the rotating basis. We will surely try to test this when we will come back in the lab!

Unfortunately, the difference between the mass of the electron we computed (529 ± 2 KeV) and its accepted value (511 KeV) was about ten times the size of the statistical error. We have looked for some sources of systematic error, but we haven't found any which would explain the right shift in the slope. This unfruitful search taught us the humility of the experimental physicist! We can find consolation in the fact that we learned a lot about modern physics experimental methods. And it could be that we still have to learn a lot about error estimates!

6 Acknowledgments

We would like to thank Fritz Buchinger for his constant help during the lab, Mark Sutton for his advices on LaTeX, Michel Beauchamp for the ton of documentation he gave us, and Saverio Biunno for his IT support and his moral presence a certain Sunday afternoon...

[8] See [6, p.68] for the theory and [3, D-2] for the values.

A Analysis of Gaussian fit method

We discuss in this appendix the details of our Gaussian fitting implementation to analyze the Compton peaks.

A.1 The Choices

First of all we needed to choose which parameter to put in our Gaussian. We decided to use the model $ae^{\frac{-(x-c)^2}{2b^2}}$ (x is the variable) without any vertical constant so that we would always obtain positive values for the modelled peak. This way, c would give us directly the peak position (it's x-average) and b would give us its standard deviation which is useful for determining the region of integration. It is worth to mention that we had first used the model $ae^{-b(x-c)^2}$, but since the standard deviation of our peaks was of the order of 200 channels, b was taking very small values and it seems that the Matlab `nlinfit` function had a hard time to converge to a pertinent value of b because of that.

Also, we needed to choose some *systematic* way to fit only the relevant part of the Compton peak with the Gaussian. We decided to consider only a certain region around the maximum. The compromise we need to do here is to choose a region big enough so that the fitting is meaningful, but small enough so that we don't fit also into background noise. The way we implemented that was by finding the maximum value of the number of counts (which is a good approximation to the peak position), and then browsing to the right and left by packets of 10 channels to check when the average of the counts in the packet had dropped to a threshold value defined by `frac`$\cdot$`max`, where `frac` is a variable parameter we can choose (see section A.3 for the code). After some trial and error, we found that a value 0.30 for `frac` was giving the best results in terms of a relevant shape for the Compton peaks. On the other hand, we needed a bigger fraction to be able to analyze the Barium spectrum since many peaks were close. The performance of the method is well demonstrated in figure 11, where a value of 0.70 was used to be able to isolate only the peak to the right.

A.2 Estimation of the error

Something we needed to check was if our results were very sensitive about which value of `frac` we were using. A comparison table is given in table 2. The peaks values derived with different fractions for the Gaussian fit are given. We can also mention that we have tried a quadratic fit $(-a*(x-c)^2+b)$ for another comparison. The results were 514 ± 6 for the mass of electron and 664 ± 8 for the γ-ray energy. The quadratic fit gives thus a better value of the mass of electron, but the statistical errors have tripled so we could think that they give less relevant results. On the other hand, the results for the Gaussian are all in the small range of 527 ± 2 KeV. So we see that the results don't depend strongly on which fraction of the peak we use to fit the data; but they do depend slightly about which model (quadratic, Gaussian, etc.) we use. This means that we truly found a stable and systematic method.

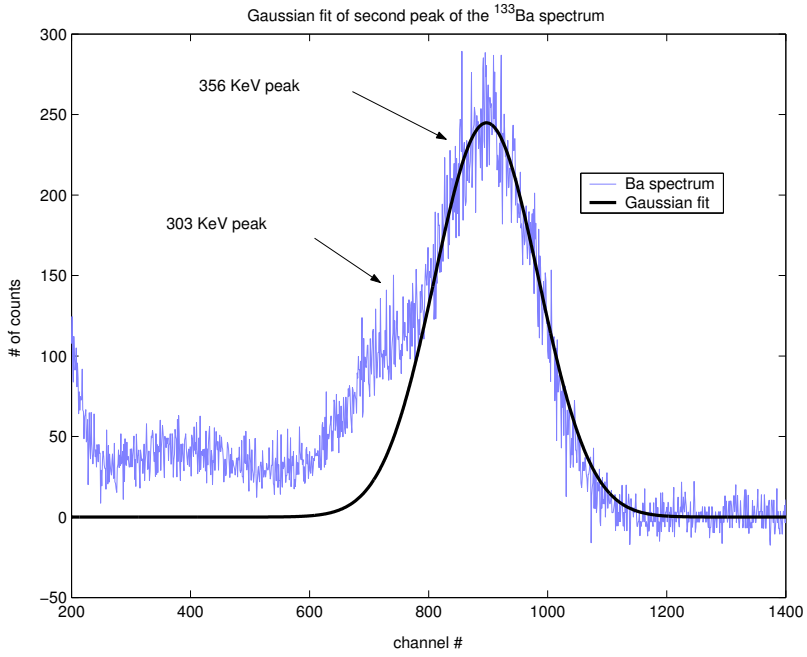

Figure 11: **Gaussian fit of the second peak of the Barium.** This spectrum had received the efficiency correction.

Comparison of different methods to measure the Compton peaks and their integral

Method	By Eye on Screen	Gaussian 0.30 without eff. Correction		Gaussian 0.10		Gaussian 0.20		Gaussian 0.30		Gaussian 0.40		Gaussian 0.50		Standard Deviation on Sums
Angle °	Peak # of counts	Peak # of counts	Sum #	Peak # of counts	Sum #	Peak # of counts	Sum #	Peak # of counts	Sum #	Peak # of counts	Sum #	Peak # of counts	Sum #	
20	1490 ± 20	1548 ± 5	18164	1559 ± 4	68832	1558 ± 5	71003	1557 ± 5	72461	1557 ± 7	73165	1552 ± 13	78630	3647
30	1423 ± 20	1433 ± 4	15616	1442 ± 3	56246	1443 ± 3	56114	1442 ± 4	56498	1444 ± 5	55820	1444 ± 6	59035	1305
40	1282 ± 20	1291 ± 4	12636	1300 ± 3	42460	1301 ± 3	41290	1300 ± 4	41388	1301 ± 5	41235	1300 ± 6	44189	1265
50	1150 ± 20	1151 ± 3	11463	1157 ± 3	33487	1159 ± 3	33064	1159 ± 3	32821	1158 ± 4	32341	1158 ± 5	32201	527
60	1010 ± 20	1022 ± 3	9961	1029 ± 2	25598	1030 ± 3	25212	1030 ± 3	25355	1029 ± 4	25125	1030 ± 5	25770	269
70	896 ± 20	902 ± 3	9408	909 ± 3	21100	910 ± 3	20580	909 ± 3	20878	909 ± 4	21236	908 ± 4	20042	475
80	795 ± 20	806 ± 3	8556	810 ± 3	17400	811 ± 3	16819	812 ± 3	16771	811 ± 4	17028	811 ± 5	17360	294
90	714 ± 20	720 ± 3	8687	722 ± 3	16164	725 ± 3	15231	726 ± 3	14990	726 ± 4	15116	724 ± 5	14779	534
100	641 ± 20	651 ± 3	8660	653 ± 3	14737	655 ± 2	14180	656 ± 2	13841	656 ± 3	13660	657 ± 3	12938	664
110	584 ± 20	596 ± 2	9282	598 ± 3	14375	599 ± 2	13786	600 ± 2	13865	598 ± 3	14424	597 ± 4	14090	289
120	500 ± 20	546 ± 3	9511	546 ± 3	14710	550 ± 3	13403	550 ± 3	13278	551 ± 4	13570	548 ± 5	12497	796
mass	513 ± 3	525.6 ± 1.4		525.3 ± 2.0		527.7 ± 1.7		529.0 ± 1.7		527.3 ± 1.7		527.0 ± 2.2		
γ energy	656 ± 4	654.6 ± 1.8		660.4 ± 2.6		660.2 ± 2.2		659.4 ± 2.1		660.3 ± 2.1		660.3 ± 2.7		

average relative error on sum	3.0%

Table 2: **Comparison in peak determination using different fractions in the Gaussian fitting.** The mass is the mass of the electron in KeV. We have left 2 digits for the errors so that we can compare it for different methods. The peaks found on spectra without efficiency correction are also shown here for comparison. Note that there is a shift of about 10 channels.

A.3 Matlab Code

This is the main function we were using in the code to analyze systematically the spectra.

```
function [param,r,j] = findPeak(X,Y, frac)
%[param r j] = findPeak(X,Y, frac) uses the data [X,Y] (each are
%vectors of same size) to find the maximum value in the Y vector
%and to isolate a region around it s.t. most of the y-values are
%above frac*maximum.
%It then runs nlinfit on this region with the Gaussian
%a*exp((x-c)^2 / (2*b^2)), ([a b c] are the parameters)
%and returns the same thing as nlinfit (param is the found
%parameters array, r & j gives information about the distribution
%of errors)

N = length(X);

%find max
imax = 1; %index of maximum
max = Y(1);
for i = 2:N
    if Y(i) >= max
        max = Y(i);
        imax = i;
    end
end

%find interval around max: look for a drop to frac of max;
%but consider packet of 10 and average them to have more stable results...
threshold = frac*max;

%browsing to the right
running = 1;
i = imax;
pack = 1:10; %hold the packets of 10 we'll browse...
right = imax; %will hold right end of interval

while(running)
    if i > N - 9
        right = N;
        break %exits while loop because reached end of array
    end
    pack = Y(i:(i+9)); %initialize packet
    if mean(pack) < threshold
        right = i + 4; %take 'middle' of pack
```

```
        running = 0; %to exit loop
    else
        i = i+1;
    end
end

%browsing to the left
running = 1;
i = imax;
pack = 1:10; %hold the packets of 10 we'll browse...
left = imax; %will hold left end of interval

while(running)
    if i < 10
        left = 1;
        break %exits while loop because reached end of array
    end
    pack = Y((i-9):i); %initialize packet
    if mean(pack) < threshold
        left = i - 4; %take 'middle' of pack
        running = 0; %to exit loop
    else
        i = i-1;
    end
end

%guessing parameters for Gaussian:
a = max;
b = (X(right)-X(imax))*frac/0.3;  %(approximation to standard deviation;
                                  %30% should lie outside both intervals)
c = X(imax); %expected average

%fitting the Gaussian
[param r j] = nlinfit(X(left:right), Y(left:right), 'Gaussian', [a b c]);
```

The following function was used in the above code.

```
function y = Gaussian(beta, x)
% Model a Gaussian exponential to be use with non-linear regression, for example.
% y = Gaussian(beta, x) where beta is a vector of parameters [a b c];
% returns a*exp(-(x-c)^2 / (2*b^2));  Note that x can be a vector if you want!

a = beta(1); b = beta(2); c = beta(3);

y = a*exp(-(x-c).^2 / (2*b^2));
```

References

[1] Birks, J.B., *The Theory of Scintillation Counting*, Pergamon Press, Oxford, 1964 3.2

[2] Frank, J., *Modern Physics*, McGraw Hill, New York, 1992 1

[3] Browne, Edgardo and Richard B. Firestone, *Table of Radioactive Isotopes*, John Wiley & Sons, 1986 4, 8

[4] Heitler, W., *The Quantum Theory of Radiation*, 3^{rd} ed., Oxford University Press 2.2

[5] Jackson, John D., *Classical Electrodynamics*, 3^{rd} ed., John Wiley & Sons, 1999 2

[6] Knoll, Glenn F., *Radiation Detection and Measurement*, John Wiley & Sons, 1979 8

[7] Melissinos, Adrian C., *Experiments in Modern Physics*, Academic Press, New York, 1966 2.2, 3

[8] Serway, Raymond A., *Optique et Physique moderne*, 4^th edition, Groupe Educalivres, 1994 2